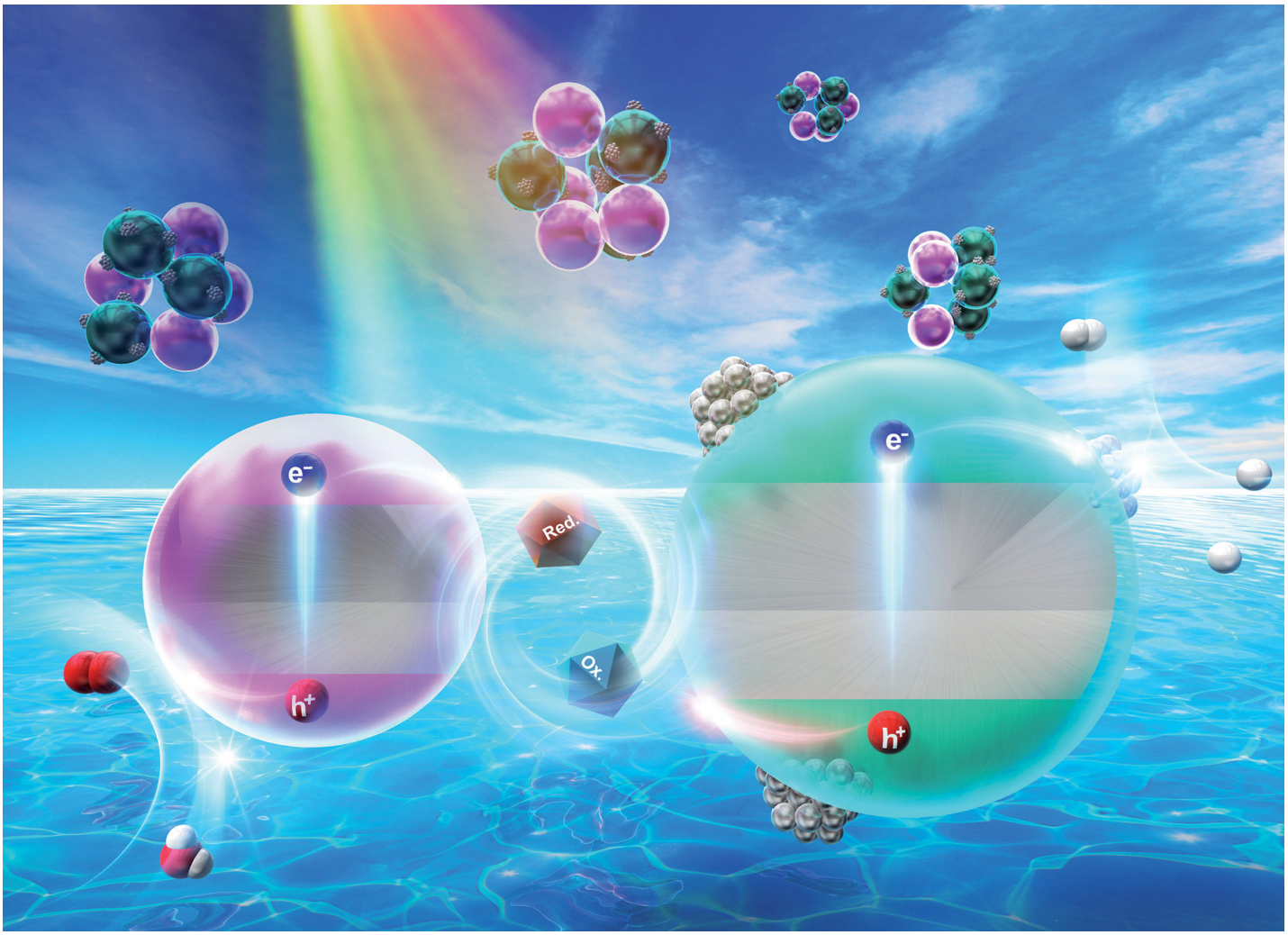

Showcasing research from Prof. Yuichi Negishi's laboratory, Tokyo University of Science, Japan

Activation of hydrogen-evolution reactivity in an Rh-doped $SrTiO_3$ photocatalyst under visible-light irradiation by loading with controlled platinum nanoclusters

Rhodium-doped strontium titanate ($SrTiO_3$:Rh)-based photocatalysts have long been studied because they can produce hydrogen (H_2) from abundant visible light and water in Z-scheme water-splitting systems. Further improvement of the H_2-evolution reaction (HER) activity of $SrTiO_3$:Rh is desired to enhance Z-scheme water splitting. In this study, we established the synthesis method of hydrophilic ~1 nm platinum nanoclusters (Pt NCs) using a ligand-exchange method while maintaining the geometric structure, and loaded method the Pt NCs onto $SrTiO_3$:Rh. The Pt NC-loaded $SrTiO_3$:Rh exhibited HER activity that is 30% higher than the Pt cocatalyst-loaded $SrTiO_3$:Rh prepared using the conventional photodeposition method.

As featured in:

See Tokuhisa Kawawaki, Yuichi Negishi *et al.*, *Energy Adv.*, 2023, **2**, 1148.

ROYAL SOCIETY OF CHEMISTRY

rsc.li/energy-advances

Registered charity number: 207890

Energy Advances

ROYAL SOCIETY OF CHEMISTRY

PAPER

View Article Online
View Journal | View Issue

Cite this: *Energy Adv.*, 2023, 2, 1148

Activation of hydrogen-evolution reactivity in an Rh-doped $SrTiO_3$ photocatalyst under visible-light irradiation by loading with controlled platinum nanoclusters†

Daichi Yazaki,[a] Tokuhisa Kawawaki,*[ab] Tomoya Tanaka,[a] Daisuke Hirayama,[a] Yamato Shingyouchi[a] and Yuichi Negishi*[ab]

Received 12th April 2023,
Accepted 7th June 2023

DOI: 10.1039/d3ya00159h

rsc.li/energy-advances

Rhodium-doped strontium titanate ($SrTiO_3$:Rh)-based photocatalysts have long been studied because they can produce hydrogen (H_2) from visible light and water in Z-scheme water-splitting systems. However, the H_2-evolution reaction (HER) of $SrTiO_3$:Rh is the rate-limiting step in such a system, so further improvement of the HER activity of $SrTiO_3$:Rh is desired to enhance Z-scheme water splitting. In this study, we synthesize hydrophilic ~1 nm platinum nanoclusters (Pt NCs) using a ligand-exchange method while maintaining the geometric structure of the corresponding hydrophobic ~1 nm Pt NC, and we load the monodispersed Pt NCs onto $SrTiO_3$:Rh. The Pt NC-loaded $SrTiO_3$:Rh exhibits HER activity that is 30% higher than that of the Pt cocatalyst-loaded $SrTiO_3$:Rh prepared using the conventional photodeposition method. This work also demonstrates that Z-scheme water splitting proceeds stoichiometrically using the Pt NC-loaded $SrTiO_3$:Rh as the H_2-evolution photocatalyst, bismuth vanadate as an oxygen-evolution photocatalyst, and Fe^{2+} as a mediator.

1. Introduction

The improvement of water-splitting photocatalysts that can produce hydrogen (H_2) from water and sunlight may greatly contribute to the establishment of next-generation sustainable energy systems.[1] In recent years, researchers have actively pursued the development of photocatalysts that can respond to visible light, which accounts for approximately 40% of the solar energy spectrum.[2–4] In particular, rhodium-doped strontium titanate[5] ($SrTiO_3$:Rh; *i.e.*, STO:Rh) is known as a visible-light-driven photocatalyst that exhibits remarkable activity in the H_2-evolution reaction (HER). The visible-light absorption of STO:Rh is attributed to a transition from the electron donor level formed by Rh^{3+} to the conduction band consisting of Ti 3d orbitals. This allows the STO:Rh to absorb visible light up to a wavelength of ~520 nm, enabling H_2 production by water splitting using not only ultra-violet light but also visible light.[5–10] For example, lanthanum (La) and Rh co-doped $SrTiO_3$ (STO:La/Rh[7,8,11–14]), which prevents Rh^{4+} substitution at Ti^{4+} sites, has achieved a quantum yield of 33% at visible light region and a solar-to-H_2 efficiency of > 1% with the use of photocatalytic sheets.[15]

Notably, STO:Rh-based H_2-evolution photocatalysts (HEPs) can achieve water splitting under visible light when combined with oxygen (O_2)-evolution photocatalysts (OEPs) to form a Z-scheme system (Fig. 1A).[16–18] For the construction of Z-scheme systems, STO:Rh-based HEP has been combined with OEPs such as TiO_2-rutile,[10] $BiVO_4$,[9,10,13,15,19,20] $SrTiO_3$:Rh/Sb,[21] $AgNbO_3$,[10] Bi_2MoO_6,[10] TiO_2:Cr/Sb,[10] TiO_2:Rh/Sb,[10] WO_3,[10,19] Ta_3N_5,[22] Bi_4NbO_8Cl,[23,24] $La_{0.5}Sr_{0.5}Ta_{0.5}Ti_{0.5}O_2N$,[25] *etc.* However, in numerous reports of Z-scheme water splitting using STO:Rh-based HEP, the HER is the rate-limiting step that suppresses the water-splitting activity. Thus, further improvement of the HER activities of STO:Rh-based HEP is desired to enhance the activity of various Z-scheme water-splittings.[9,11]

The water-splitting photocatalyst is generally composed of a photocatalyst support and metal/metal oxide nanoparticles (NPs) that function as cocatalysts. In the development of highly active photocatalysts, not only the improvement of the photocatalyst support but also the improvement of the cocatalyst, which works as the actual reaction site, is necessary. The cocatalysts are mainly loaded using the photodeposition[26] (PD, Fig. 1Ba) and impregnation

[a] *Department of Applied Chemistry, Faculty of Science, Tokyo University of Science, 1-3 Kagurazaka, Shinjuku-ku, Tokyo 162–8601, Japan. E-mail: kawawaki@rs.tus.ac.jp, negishi@rs.tus.ac.jp*
[b] *Research Institute for Science and Technology, Tokyo University of Science, 2641 2641 Yamazaki, Noda, Chiba, 278–8510, Japan*

† Electronic supplementary information (ESI) available: Experimental section, and experimental, characterization, peak assignments of FT-IR, additional figures, characterization of Pt NCs, additional UV-Vis, XPS, FT-IR and FT-EXAFS spectra, SEM and TEM images, and photocatalytic activity. Correspondence and requests for materials should be addressed to T.K. and Y.N. See DOI: https://doi.org/10.1039/d3ya00159h

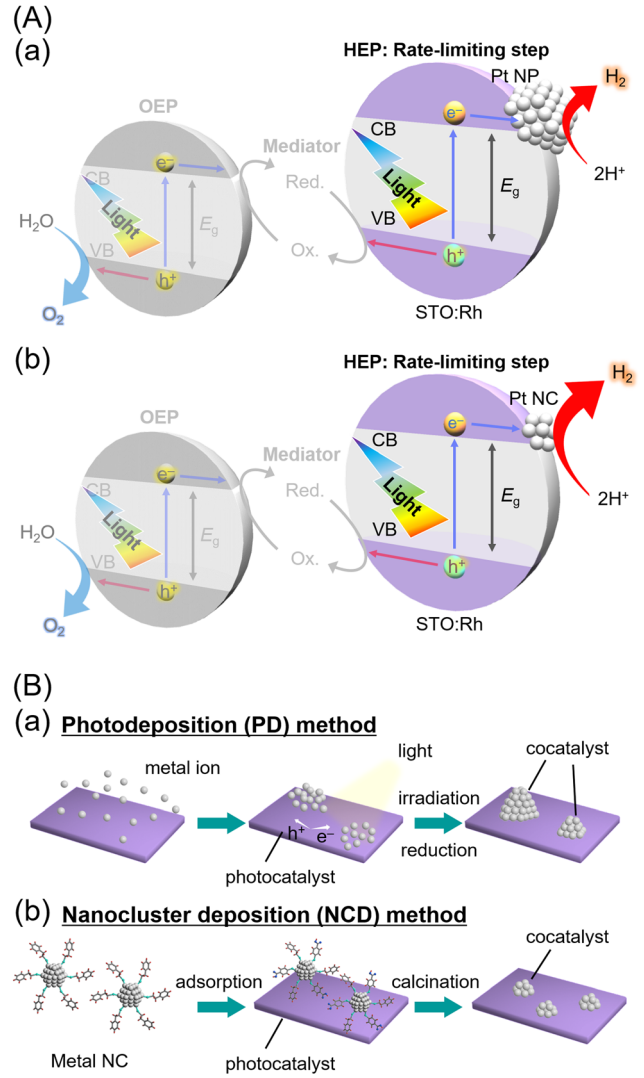

Fig. 1 Schematic illustrations of (A) Z-scheme photocatalytic water splitting and (B) the preparation procedure of cocatalysts on the photocatalysts using the (a) conventional PD method and (b) NCD method. In (A), CB, conduction band; VB, valence band; E_g, band gap; Red, reductants; and Ox, oxidants. STO:Rh is one of the most advanced HEP. The improvement in water-splitting activity can be expected by enhancing the reaction in HEPs, which is the rate-limiting step.

methods.[27] Although these methods are simple, it is difficult to control the particle size and electronic state of the cocatalyst particles. Therefore, the improvement of cocatalyst-loading methods[28–32] has also been actively studied to enhance water-splitting activity. In particular, the method[33–36] of loading metal NPs with controlled size and chemical composition, which are prepared by liquid-phase synthesis, onto a photocatalyst is effective in controlling the particle size and electronic state of the cocatalyst.[37–41] Furthermore, metal nanoclusters (NCs) with diameters of ~1 nm have unique properties compared with those of metal NPs (diameters > ~2 nm) and bulk metals. The NC deposition (NCD, Fig. 1Bb) method, which exploits the unique characteristics of metal NCs, can create a cocatalyst surface that is more favorable for the adsorption of the substrate and the desorption of the products, resulting in enhanced activity in the water-splitting reaction. The use of atomically precise gold (Au) NCs,[38,42,43] ~1 nm Au–platinum (Pt) alloy NCs,[44] rhodium–chromium mixed oxide ($Rh_{2-x}Cr_xO_y$) NCs,[45] $Pt_{\sim 51}$ NCs,[46] ~1.4 nm Pt–ruthenium (PtRu),[47] and Au NCs[48] as cocatalysts has led to improved water-splitting and HER activity.

In this study, we attempted to further improve the HER activity of STO:Rh by employing fine Pt NCs as a cocatalyst. To this end, we established a method to load Pt NCs on STO:Rh, which has a hydrophilic surface, with a high adsorption yield by applying an appropriate hydrophilic treatment to the Pt NCs. As a result, the H_2-evolution efficiency of STO:Rh was increased by 30% compared with that of the Pt-cocatalyst-loaded STO:Rh prepared using the conventional PD method. Additionally, stoichiometric overall water splitting was successfully achieved using Pt NC-loaded STO:Rh as the HEP in Z-scheme water splitting.

2. Results and discussion

2.1. Preparation of Pt NC-loaded $SrTiO_3$:Rh

The STO:Rh was prepared by solid-state reaction with 1 mol% of Rh doping, according to a previous report.[5] The Brunauer–Emmett–Teller surface area of STO:Rh (Fig. S1, ESI†) was estimated to be 2.5 $m^2\ g^{-1}$ (Table S1, ESI†) and powder X-ray diffraction (PXRD) indicated relatively high crystallinity of the product (Fig. S2, ESI†). The strong visible-light absorption was confirmed by ultraviolet-visible (UV-Vis) absorption spectroscopy. These results confirmed that the desired STO:Rh was obtained (Fig. S2, ESI†).

The $Pt_{\sim 51}$ NC protected by 2-phenylethanethiolate (PET) and carbon monoxide (CO) ($Pt_{\sim 51}(PET)_n(CO)_m$) was synthesized by combining polyol reduction with ligand exchange, similar to our previous report.[49] Unfortunately, the obtained $Pt_{\sim 51}(PET)_n(CO)_m$ cannot efficiently adsorb on the hydrophilic surface of STO:Rh because the PET ligands are hydrophobic. Therefore, parts of the ligands on the Pt NCs were replaced by *p*-mercaptobenzoic acid (*p*-MBA), which has a hydrophilic carboxylic acid group but a similar framework structure to PET.[44] Fourier transform infrared (FT-IR) spectra were obtained before and after ligand exchange (Table S2, ESI†), as shown in Fig. S3a (ESI†). The spectra of these modified NCs after ligand exchange showed peaks attributed to the C–OH stretching and O–H···O bending vibrations in *p*-MBA (1427.1, 1326.8, and 927.6 cm^{-1}),[50] which confirmed that ligand exchange proceeded. No significant changes occurred in the matrix-assisted laser desorption ionization mass (MALDI-MS) spectra (Fig. S3b, ESI†), UV-Vis absorption spectra (Fig. S3c, ESI†), Pt L_3-edge X-ray absorption near edge structure (XANES) spectra (Fig. S5a, ESI†), or Fourier transform-extended X-ray absorption fine structure (FT-EXAFS) spectra (Fig. S5b, ESI†) before and after ligand exchange. These results suggest that many ligands were replaced from PET to *p*-MBA while maintaining the structure of the Pt NCs. The Pt NCs obtained by ligand exchange ($Pt_{\sim 51}(PET)_n(CO)_m(p\text{-MBA})_l$) showed high solubility in polar solvents such as methanol and acetone (Fig. S4 and Table S3, ESI†).

However, they were not soluble in water, which is a highly polar solvent, indicating that not all PET ligands were replaced by *p*-MBA, and some PET ligands remained on the surfaces of the Pt NCs.

The obtained $Pt_{\sim 51}(PET)_n(CO)_m(p\text{-MBA})_l$ was dispersed in tetrahydrofuran and stirred with STO:Rh for 3 h to adsorb on the STO:Rh surface. A 96% adsorption yield was achieved, which is higher than that of Pt NCs without ligand exchange ($Pt_{\sim 51}(PET)_n(CO)_m$, 73%), due to the formation of hydrogen bonds between the carboxylic acid group (–COOH) of the *p*-MBA ligands on $Pt_{\sim 51}(PET)_n(CO)_m(p\text{-MBA})_l$ and the hydroxyl group (–OH) on STO:Rh.[44,48] However, the presence of ligands suppresses the accessibility of a substance and the efficiency of electron transfer from the photocatalysts to the NCs, which leads to a decrease in catalytic activity. Therefore, the obtained $Pt_{\sim 51}(PET)_n(CO)_m(p\text{-MBA})_l$-loaded STO:Rh ($Pt_{\sim 51}(PET)_n(CO)_m(p\text{-MBA})_l$/STO:Rh) was calcined at 300 °C under reduced pressure to remove most of the ligands from the Pt NC surface (Pt_{NC}/STO:Rh). The calcination temperature (300 °C) was determined based on the desorption temperature of the ligands in the thermogravimetric analysis of Pt NCs.[49]

Fig. 2 shows the Pt L_3-edge FT-EXAFS spectra of Pt NC and Pt NC-loaded STO:Rh in each preparation process (Fig. S6, ESI†). The peak located at approximately 2.0 Å, which is attributed to the Pt–S bond, was observed in both $Pt_{\sim 51}(PET)_n(CO)_m(p\text{-MBA})_l$ and $Pt_{\sim 51}(PET)_n(CO)_m(p\text{-MBA})_l$/STO:Rh. In the spectrum of Pt_{NC}/STO:Rh, the Pt–S bond was not observed, and instead, a peak (~1.8 Å) attributed to the Pt–O bond was observed (Fig. 2). This suggests that most of the S species in the ligands were desorbed from Pt NC by the calcination process through Pt–S dissociation. The S $2p_{3/2}$ X-ray photoelectron spectroscopy (XPS) spectrum of Pt_{NC}/STO:Rh (Fig. S7, ESI†) shows a peak attributed to a S species in a highly oxidized state. These results indicate that most of the S remains on STO:Rh after desorption from Pt NC surfaces, mainly as SO_4^{2-} (Fig. S7, ESI†).[48] Transmission electron microscopy (TEM) images (Fig. 3a) indicated that the average particle size of the Pt NC cocatalyst (Pt_{NC}) in Pt_{NC}/STO:Rh was 1.5 ± 0.3 nm. This indicates that there was effectively no significant aggregation of $Pt_{\sim 51}$ during calcination and it was presumed that 92.8% of $Pt_{\sim 51}$ on Pt_{NC}/STO:Rh has a three-dimensional structure after the calcination (Fig. S8 and S9, ESI†). Therefore, fine and monodispersed Pt NCs were loaded on STO:Rh (Fig. 3a).

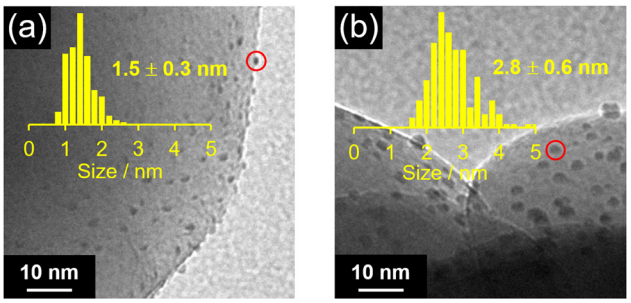

Fig. 3 TEM images and resulting histograms (inset) for the particle-size distribution of Pt cocatalysts in (a) Pt_{NC}/STO:Rh and (b) Pt_{PD}/STO:Rh.

We also used the PD method to load a Pt cocatalyst (Pt_{PD}) on STO:Rh (Pt_{PD}/STO:Rh). As a result, Pt_{PD} with an average particle size of 2.8 ± 0.6 nm was loaded on STO:Rh (Fig. 3b). This indicates that Pt cocatalysts with high monodispersity but about half the particle size can be obtained using our method (Pt_{NC}/STO:Rh) compared with the PD method (Pt_{PD}/STO:Rh). Assuming that the loaded Pt_{NC} and Pt_{PD} have a face-centered cubic structure, Pt_{NC} was estimated to have 1.58 times more active sites (*i.e.*, Pt atoms on the surfaces of Pt cocatalysts) than Pt_{PD} (Table S4, ESI†).

The obtained Pt_{NC} in Pt_{NC}/STO:Rh was more oxidized than that in $Pt_{\sim 51}(PET)_n(CO)_m(p\text{-MBA})_l$ and $Pt_{\sim 51}(PET)_n(CO)_m(p\text{-MBA})_l$/STO:Rh (Fig. 2 and 4). This means that oxidation of

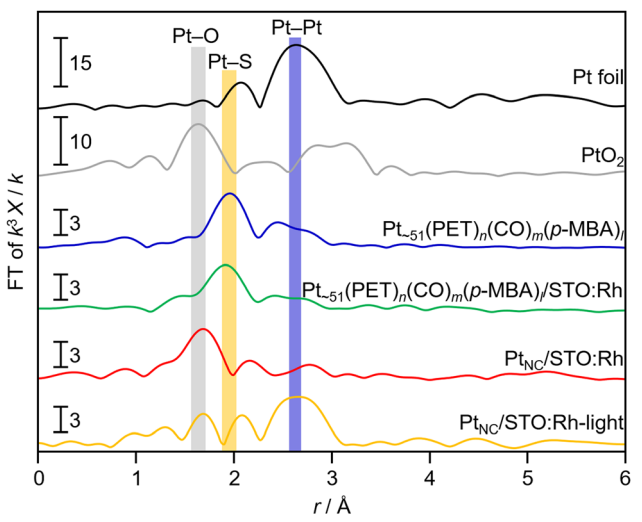

Fig. 2 Pt L_3-edge FT-EXAFS spectra of $Pt_{\sim 51}(PET)_n(CO)_m(p\text{-MBA})_l$, before ($Pt_{\sim 51}(PET)_n(CO)_m(p\text{-MBA})_l$/STO:Rh) and after ($Pt_{NC}$/STO:Rh) calcination of Pt NC-loaded STO:Rh, and after light irradiation of Pt_{NC}/STO:Rh (Pt_{NC}/STO:Rh-light). Pt foil and PtO_2 powder are also shown for comparison.

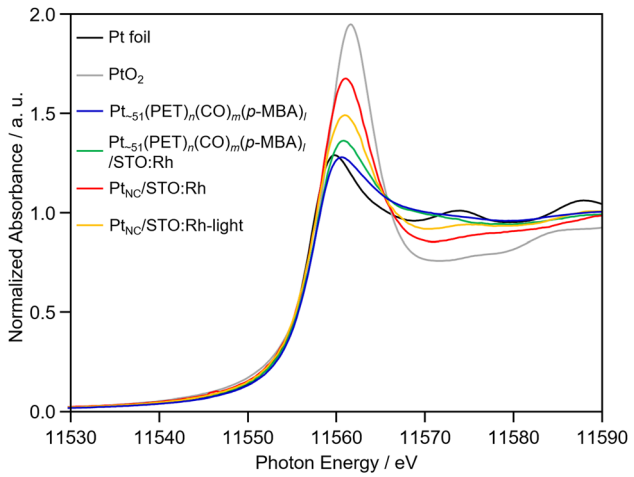

Fig. 4 Pt L_3-edge XANES spectra of $Pt_{\sim 51}(PET)_n(CO)_m(p\text{-MBA})_l$, before ($Pt_{\sim 51}(PET)_n(CO)_m(p\text{-MBA})_l$/STO:Rh) and after ($Pt_{NC}$/STO:Rh) calcination of Pt NC-loaded STO:Rh, and after light irradiation onto Pt_{NC}/STO:Rh (Pt_{NC}/STO:Rh-light). Pt foil (Pt^0) and PtO_2 powder (Pt^{4+}) were also shown for comparison. A stronger and weaker absorbance indicates a more oxidized and reduced electronic state of Pt at the whiteline, respectively.

the Pt NCs occurred during calcination. Therefore, we attempted to reduce Pt_{NC} with photoexcited electrons produced by irradiating the Pt_{NC}/STO:Rh dispersed in water (Pt_{NC}/STO:Rh-light). As a result, Pt_{NC} was significantly reduced and a strong Pt–Pt bond was observed (Fig. 2 and 4). Accordingly, the peaks attributed to the S species were significantly decreased in the S $2p_{3/2}$ XPS spectrum of Pt_{NC}/STO:Rh-light compared with Pt_{NC}/STO:Rh before light irradiation (Fig. S7, ESI†). This means that SO_4^{2-} and other residues on the STO:Rh surface were removed by washing or oxidative desorption after photoirradiation in water. The PXRD patterns, Rh K-edge XANES spectra, FT-IR spectra, and scanning electron microscopy images of the samples (Fig. S1, S2, and S10, ESI†) confirmed that no change occurred in the STO:Rh during the series of operations required for this Pt NC-loading even except for only a charge state of Rh. The slightly oxidized electronic state of Rh by the calcination process was reduced by light irradiation (Fig. S11, ESI†). From these results, we concluded that Pt NCs with metallic electronic states were successfully loaded on STO:Rh with relatively fine and monodispersed particle sizes.

2.2. H_2-evolution activity of Pt NC-loaded $SrTiO_3$:Rh

Next, we evaluated the photocatalytic activity of Pt_{NC}/STO:Rh. To estimate the function of Pt_{NC} as an HER cocatalyst more accurately, H_2-evolution activity was evaluated in a half-reaction with methanol as a hole sacrificial agent (Fig. S12, ESI†). For comparison, the same measurements were performed for Pt_{PD}/STO:Rh.

First, we investigated the effect of ligand removal by calcination on H_2-evolution activity (Fig. 5a). From the comparison with Pt_{NC}/STO:Rh before and after calcination, we confirmed that the H_2-evolution activity increased by ~80 times after the calcination treatment. The removal of ligands from the Pt_{NC} surface contributes to this improvement by making it easier for protons to approach the Pt_{NC} cocatalyst and enhancing electron transfer from STO:Rh to the Pt_{NC} cocatalyst. For comparison, H_2-evolution activity was also measured for Pt_{PD}/STO:Rh, in which the Pt cocatalyst was loaded on STO:Rh pre-calcined at 300 °C using the PD method. As a result, almost no change in the activity of Pt_{PD}/STO:Rh was observed (Fig. S13, ESI†). This indicates that the calcination treatment did not affect the activity of the photocatalyst support (*i.e.*, STO:Rh), and the increase in activity is mainly attributed to the removal of ligands from the surface of the Pt_{NC} cocatalyst.

Next, we investigated the effect of the amount of Pt loading on activity (Fig. 5b). The results showed that the maximum activity was obtained at a loading of 0.4 wt% Pt. Comparing the H_2-evolution activity of Pt_{NC}/STO:Rh and Pt_{PD}/STO:Rh when they were both loaded using 0.4 wt% Pt, Pt_{NC}/STO:Rh showed 30% higher H_2-evolution rate than Pt_{PD}/STO:Rh (Fig. 5c and Fig. S14, ESI†). Considering the results of the Pt L_3-edge XANES analysis, there is no significant difference in the electronic state of the Pt cocatalyst between Pt_{NC}/STO:Rh and Pt_{PD}/STO:Rh (Fig. S15, ESI†). This suggests that the difference in activity between Pt_{NC}/STO:Rh and Pt_{PD}/STO:Rh is mainly due to the increase in the number of active sites for the reaction, which was enabled by decreasing the size of the Pt cocatalyst (Table S4, ESI†). To eliminate the dependence of a hole sacrificial agent, we evaluated H_2-evolution activity using $FeCl_2$. The Pt_{NC}/STO:Rh shows higher activity than Pt_{PD}/STO:Rh and it was indicated that $FeCl_2$

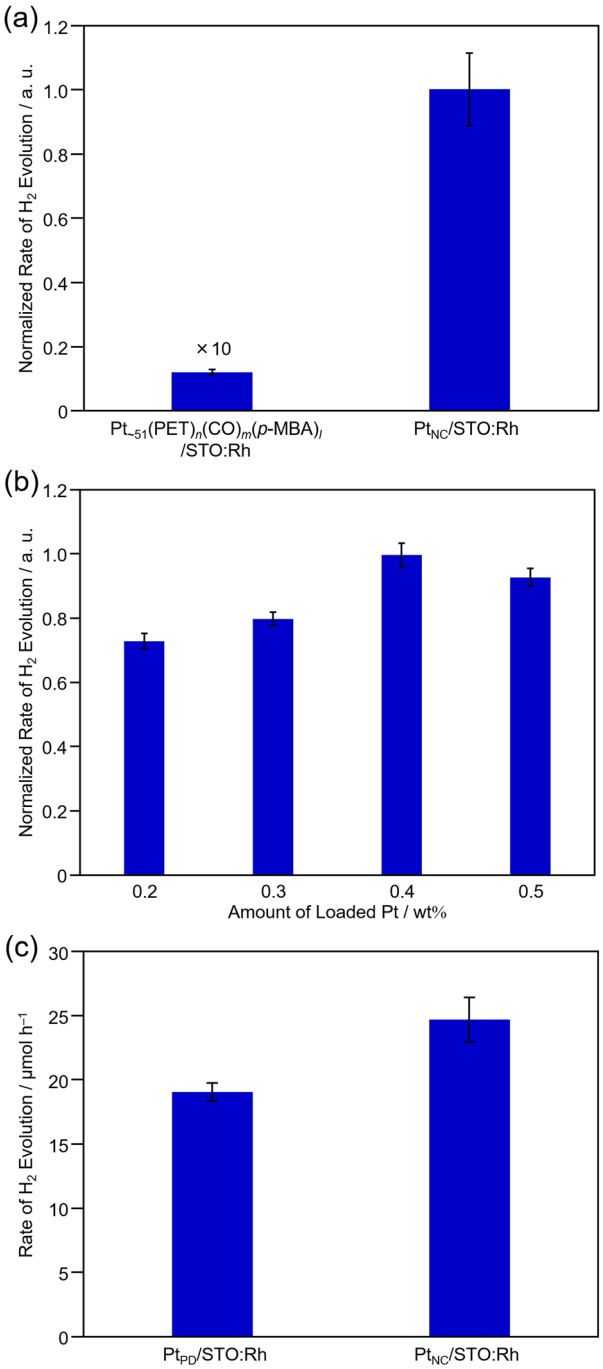

Fig. 5 H_2-evolution activity of Pt cocatalyst-loaded STO:Rh photocatalysts. (a) Before ($Pt_{\sim 51}(PET)_n(CO)_m(p\text{-MBA})_l$/STO:Rh) and after ($Pt_{NC}$/STO:Rh) calcination of Pt NC-loaded STO:Rh and (b) dependence of loading weight of the Pt cocatalyst for Pt_{NC}/STO:Rh. (c) Comparison of H_2-evolution activity between Pt_{NC}/STO:Rh and Pt_{PD}/STO:Rh. In (a) and (c), the loading weight of Pt on them was 0.4 wt%. In order to eliminate the effect of the difference in the activity of each photocatalyst, STO:Rh synthesized in the same batch was used in each experiment (a)–(c).

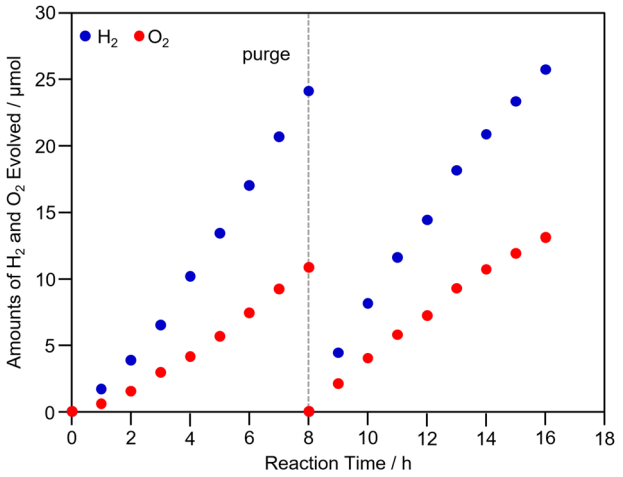

Fig. 6 Time course of water-splitting activity for the Pt_{NC}/STO:Rh-$BiVO_4$ composite Z-scheme system using $FeCl_2$ as a mediator. Light source: a 300 W Xe lamp with a long-pass filter (> ~410 nm), catalyst: 100 mg for each catalyst, reactant solution: 120 mL of 2 mmol L^{-1} $FeCl_2$ in H_2SO_4 aq. (pH 2.4), reaction cell: a top-window reaction cell.

works as a mediator for Z-scheme water splitting (Fig. S16, ESI†).

Finally, we attempted Z-scheme water splitting using Pt_{NC}/STO:Rh. In this experiment, Pt_{NC}/STO:Rh was used as the HEP, $BiVO_4$ as the OEP, and Fe^{2+} or Fe^{3+} as a mediator.[9,19,51,52] First, the water-splitting activity obtained using Fe^{3+} is shown in Fig. S17 (ESI†). In this case, O_2 was produced in excess and stoichiometric H_2 and O_2 evolution was not observed ($H_2:O_2$ ratio = 1.65 at 16 h light irradiation). This suggests that excess Fe^{3+} prevented H_2 evolution in Pt_{NC}/STO:Rh. Next, we evaluated the water-splitting activity using Fe^{2+} as a mediator (Fig. 6). After a slight induction period, stoichiometric H_2 and O_2 evolution was observed ($H_2:O_2$ ratio = 1.99 at 16 h light irradiation). In this case, stable gas evolution was observed even after 16 h of light irradiation, indicating that Pt_{NC}/STO:Rh is highly stable. Thus, when Pt_{NC}/STO:Rh is used for the HEP, stoichiometric Z-scheme water splitting can stably proceed when Fe^{2+} is used as a mediator. It has been reported that the Fe^{3+} chemical species generated by the addition of $FeCl_3$ in sulfuric acid solutions adsorbs on the surface of the Pt cocatalyst, preventing (1) the formation of dissociative adsorbed H_2 on the Pt cocatalyst, (2) the reverse reaction from H_2 to H_2O, and (3) minor reactions in which Fe^{3+} is reduced by H_2 (Fig. S18, ESI†).[19,52] Although there was no significant difference between the electronic structures of Pt_{NC} and Pt_{PD}, because the number of Pt atoms constituting the Pt_{NC} and Pt_{PD} cocatalysts is different, it is assumed that there is a difference in the geometric structure of the Pt cocatalysts. The adsorption of Fe^{3+} chemical species on the surface of the Pt_{NC} is likely more inhibited than that on the Pt_{PD} because of the difference in the geometric structure. Therefore, using Pt_{NC}/STO:Rh as the HEP might decrease the production of H_2 when the mediator is Fe^{3+}. Unfortunately, no significant improvement in H_2 production was observed with Pt_{NC}/STO:Rh-$BiVO_4$ compared with Pt_{PD}/STO:Rh-$BiVO_4$ in an overall water splitting using Fe^{2+} due to probably the high reactivity of Pt_{NC}/STO:Rh in terms of the side reactions and reverse reactions in the overall water-splitting reaction. Therefore, it is necessary to search for conditions for Z-scheme water-splitting suitable for the evaluation of the Pt_{NC}/STO:Rh-$BiVO_4$ as well as in the case of the Pt_{PD}/STO:Rh-$BiVO_4$.[19]

Conclusions

In this study, we loaded Pt cocatalysts with a fine particle size of 1.5 nm onto STO:Rh, which is a promising visible-light-driven photocatalyst, using pre-synthesized hydrophilic $Pt_{\sim 51}$ NCs as a precursor. The novel Pt_{NC}/STO:Rh-light photocatalyst exhibited 30% higher H_2-evolution activity than Pt_{PD}/STO:Rh. This improvement was mainly attributed to the increase in active sites when using finer Pt particles. Furthermore, by using the appropriate mediator, the Z-scheme water splitting proceeded stoichiometrically using Pt_{NC}/STO:Rh as the HEP. Although STO:Rh has been frequently used as the HEP in Z-scheme water splitting, the reaction on STO:Rh is the rate-limiting step in most cases. The method developed in this report for increasing the activity of STO:Rh may lead to further improvements in the performance of novel visible-light-driven Z-scheme water-splitting systems.

Author contributions

T. K. and Y. N. conceived the research and designed the experiments. T. K. and Y. N. designed the synthesis and photocatalytic tests. D. Y., T. T., D. H., and Y. S. performed the synthesis, characterization, and photocatalytic activity. T. K. and Y. N. wrote the manuscript.

Conflicts of interest

There are no conflicts to declare.

Acknowledgements

This work was supported by the Japan Society for the Promotion of Science (JSPS) KAKENHI (grant number 20H02698, 20H02552), Scientific Research on Innovative Areas "Innovations for Light-Energy Conversion" (grant number 18H05178 and 20H05115), Scientific Research on Innovative Areas "Hydrogenomics" (grant number 21H00027) and Joint Usage/Research Center for Catalysis (Proposal 22AY0056 and 23AY0189). Funding from the Takahashi Industrial and Economic Research Foundation, the Yazaki Memorial Foundation for Science and Technology, the Ogasawara Foundation for the Promotion of Science and Engineering, the Kao Foundation for Arts and Sciences, the Sasakawa Scientific Research Grant from the Japan Science Society, TEPCO Memorial Foundation Research Grant (Basic Research), Advanced Technology Institute Research Grants 2022 and the Kumagai Foundation for Science and Technology is gratefully acknowledged.

References

1 S. Chen, T. Takata and K. Domen, *Nat. Rev. Mater.*, 2017, **2**, 17050.
2 B. A. Pinaud, J. D. Benck, L. C. Seitz, A. J. Forman, Z. Chen, T. G. Deutsch, B. D. James, K. N. Baum, G. N. Baum, S. Ardo, H. Wang, E. Miller and T. F. Jaramillo, *Energy Environ. Sci.*, 2013, **6**, 1983–2002.
3 D. M. Fabian, S. Hu, N. Singh, F. A. Houle, T. Hisatomi, K. Domen, F. E. Osterloh and S. Ardo, *Energy Environ. Sci.*, 2015, **8**, 2825–2850.
4 T. Hisatomi, K. Takanabe and K. Domen, *Catal. Lett.*, 2015, **145**, 95–108.
5 R. Konta, T. Ishii, H. Kato and A. Kudo, *J. Phys. Chem. B*, 2004, **108**, 8992–8995.
6 S. Kawasaki, K. Akagi, K. Nakatsuji, S. Yamamoto, I. Matsuda, Y. Harada, J. Yoshinobu, F. Komori, R. Takahashi, M. Lippmaa, C. Sakai, H. Niwa, M. Oshima, K. Iwashina and A. Kudo, *J. Phys. Chem. C*, 2012, **116**, 24445–24448.
7 B. Modak and S. K. Ghosh, *J. Phys. Chem. B*, 2015, **119**, 11089–11098.
8 D. H. K. Murthy, H. Matsuzaki, Q. Wang, Y. Suzuki, K. Seki, T. Hisatomi, T. Yamada, A. Kudo, K. Domen and A. Furube, *Sustainable Energy Fuels*, 2019, **3**, 208–218.
9 H. Kato, Y. Sasaki, N. Shirakura and A. Kudo, *J. Mater. Chem. A*, 2013, **1**, 12327–12333.
10 Y. Sasaki, H. Nemoto, K. Saito and A. Kudo, *J. Phys. Chem. C*, 2009, **113**, 17536–17542.
11 Q. Wang, T. Hisatomi, S. S. K. Ma, Y. Li and K. Domen, *Chem. Mater.*, 2014, **26**, 4144–4150.
12 Q. Wang, Y. Li, T. Hisatomi, M. Nakabayashi, N. Shibata, J. Kubota and K. Domen, *J. Catal.*, 2015, **328**, 308–315.
13 Q. Wang, T. Hisatomi, Y. Suzuki, Z. Pan, J. Seo, M. Katayama, T. Minegishi, H. Nishiyama, T. Takata, K. Seki, A. Kudo, T. Yamada and K. Domen, *J. Am. Chem. Soc.*, 2017, **139**, 1675–1683.
14 B. Moss, Q. Wang, K. T. Butler, R. Grau-Crespo, S. Selim, A. Regoutz, T. Hisatomi, R. Godin, D. J. Payne, A. Kafizas, K. Domen, L. Steier and J. R. Durrant, *Nat. Mater.*, 2021, **20**, 511–517.
15 Q. Wang, T. Hisatomi, Q. Jia, H. Tokudome, M. Zhong, C. Wang, Z. Pan, T. Takata, M. Nakabayashi, N. Shibata, Y. Li, I. D. Sharp, A. Kudo, T. Yamada and K. Domen, *Nat. Mater.*, 2016, **15**, 611–615.
16 A. J. Bard, *J. Photochem.*, 1979, **10**, 59–75.
17 K. Maeda, *ACS Catal.*, 2013, **3**, 1486–1503.
18 Y. Wang, H. Suzuki, J. Xie, O. Tomita, D. J. Martin, M. Higashi, D. Kong, R. Abe and J. Tang, *Chem. Rev.*, 2018, **118**, 5201–5241.
19 H. Kato, Y. Sasaki, A. Iwase and A. Kudo, *Bull. Chem. Soc. Jpn.*, 2007, **80**, 2457–2464.
20 Q. Wang, S. Okunaka, H. Tokudome, T. Hisatomi, M. Nakabayashi, N. Shibata, T. Yamada and K. Domen, *Joule*, 2018, **2**, 2667–2680.
21 R. Niishiro, S. Tanaka and A. Kudo, *Appl. Catal., B*, 2014, **150–151**, 187–196.
22 S. S. K. Ma, K. Maeda, T. Hisatomi, M. Tabata, A. Kudo and K. Domen, *Chem. – Eur. J.*, 2013, **19**, 7480–7486.
23 H. Fujito, H. Kunioku, D. Kato, H. Suzuki, M. Higashi, H. Kageyama and R. Abe, *J. Am. Chem. Soc.*, 2016, **138**, 2082–2085.
24 K. Ogawa, A. Nakada, H. Suzuki, O. Tomita, M. Higashi, A. Saeki, H. Kageyama and R. Abe, *ACS Appl. Mater. Interfaces*, 2019, **11**, 5642–5650.
25 H. Kumagai, R. Aoyagi, K. Kato, A. Yamakata, M. Kakihana and H. Kato, *ACS Appl. Energy Mater.*, 2021, **4**, 2056–2060.
26 B. Kraeutler and A. J. Bard, *J. Am. Chem. Soc.*, 1978, **100**, 4317–4318.
27 K. Domen, S. Naito, M. Soma, T. Onishi and K. Tamaru, *J. Chem. Soc., Chem. Commun.*, 1980, **12**, 543–544.
28 Z. Wang, Y. Luo, T. Hisatomi, J. J. M. Vequizo, S. Suzuki, S. Chen, M. Nakabayashi, L. Lin, Z. Pan, N. Kariya, A. Yamakata, N. Shibata, T. Takata, K. Teshima and K. Domen, *Nat. Commun.*, 2021, **12**, 1005.
29 L. Qin, G. Si, X. Li and S.-Z. Kang, *RSC Adv.*, 2015, **5**, 102593–102598.
30 S. Y. Xiao, Y. Liu, X. F. Wu, L. T. Gan, H. Y. Lin, L. R. Zheng, S. Dai, P. F. Liu and H. G. Yang, *J. Mater. Chem. A*, 2021, **9**, 14786–14792.
31 T. Takata, J. Jiang, Y. Sakata, M. Nakabayashi, N. Shibata, V. Nandal, K. Seki, T. Hisatomi and K. Domen, *Nature*, 2020, **581**, 411–414.
32 R. Li, F. Zhang, D. Wang, J. Yang, M. Li, J. Zhu, X. Zhou, H. Han and C. Li, *Nat. Commun.*, 2013, **4**, 1432.
33 T. Kawawaki, A. Ebina, Y. Hosokawa, S. Ozaki, D. Suzuki, S. Hossain and Y. Negishi, *Small*, 2021, **17**, 2005328.
34 T. Kawawaki, Y. Kataoka, S. Ozaki, M. Kawachi, M. Hirata and Y. Negishi, *Chem. Commun.*, 2021, **57**, 417–440.
35 T. Kawawaki, Y. Mori, K. Wakamatsu, S. Ozaki, M. Kawachi, S. Hossain and Y. Negishi, *J. Mater. Chem. A*, 2020, **8**, 16081–16113.
36 T. Kawawaki, Y. Negishi and H. Kawasaki, *Nanoscale Adv.*, 2020, **2**, 17–36.
37 N. Sakamoto, H. Ohtsuka, T. Ikeda, K. Maeda, D. Lu, M. Kanehara, K. Teramura, T. Teranishi and K. Domen, *Nanoscale*, 2009, **1**, 106–109.
38 Y. Negishi, M. Mizuno, M. Hirayama, M. Omatoi, T. Takayama, A. Iwase and A. Kudo, *Nanoscale*, 2013, **5**, 7188–7192.
39 M. Luo, Y. Hong, W. Yao, C. Huang, Q. Xu and Q. Wu, *J. Mater. Chem. A*, 2015, **3**, 2770–2775.
40 S. Cao, J. Jiang, B. Zhu and J. Yu, *Phys. Chem. Chem. Phys.*, 2016, **18**, 19457–19463.
41 M. Luo, P. Lu, W. Yao, C. Huang, Q. Xu, Q. Wu, Y. Kuwahara and H. Yamashita, *ACS Appl. Mater. Interfaces*, 2016, **8**, 20667–20674.
42 W. Kurashige, R. Kumazawa, D. Ishii, R. Hayashi, Y. Niihori, S. Hossain, L. V. Nair, T. Takayama, A. Iwase, S. Yamazoe, T. Tsukuda, A. Kudo and Y. Negishi, *J. Phys. Chem. C*, 2018, **122**, 13669–13681.
43 Y. Negishi, Y. Matsuura, R. Tomizawa, W. Kurashige, Y. Niihori, T. Takayama, A. Iwase and A. Kudo, *J. Phys. Chem. C*, 2015, **119**, 11224–11232.
44 W. Kurashige, R. Hayashi, K. Wakamatsu, Y. Kataoka, S. Hossain, A. Iwase, A. Kudo, S. Yamazoe and Y. Negishi, *ACS Appl. Energy Mater.*, 2019, **2**, 4175–4187.

45 W. Kurashige, Y. Mori, S. Ozaki, M. Kawachi, S. Hossain, T. Kawawaki, C. J. Shearer, A. Iwase, G. F. Metha, S. Yamazoe, A. Kudo and Y. Negishi, *Angew. Chem., Int. Ed.*, 2020, **59**, 7076–7082.
46 D. Yazaki, T. Kawawaki, D. Hirayama, M. Kawachi, K. Kato, S. Oguchi, Y. Yamaguchi, S. Kikkawa, Y. Ueki, S. Hossain, D. J. Osborn, F. Ozaki, S. Tanaka, J. Yoshinobu, G. F. Metha, S. Yamazoe, A. Kudo, A. Yamakata and Y. Negishi, Small, in press.
47 C. M. Pelicano, M. Saruyama, R. Takahata, R. Sato, Y. Kitahama, H. Matsuzaki, T. Yamada, T. Hisatomi, K. Domen and T. Teranishi, *Adv. Funct. Mater.*, 2022, **32**, 2202987.
48 T. Kawawaki, Y. Kataoka, M. Hirata, Y. Akinaga, R. Takahata, K. Wakamatsu, Y. Fujiki, M. Kataoka, S. Kikkawa, A. S. Alotabi, S. Hossain, D. J. Osborn, T. Teranishi, G. G. Andersson, G. F. Metha, S. Yamazoe and Y. Negishi, *Angew. Chem., Int. Ed.*, 2021, **60**, 21340–21350.
49 T. Kawawaki, N. Shimizu, K. Funai, Y. Mitomi, S. Hossain, S. Kikkawa, D. J. Osborn, S. Yamazoe, G. F. Metha and Y. Negishi, *Nanoscale*, 2021, **13**, 14679–14687.
50 S. E. Creager and C. M. Steiger, *Langmuir*, 1995, **11**, 1852–1854.
51 Q. Jia, A. Iwase and A. Kudo, *Chem. Sci.*, 2014, **5**, 1513–1519.
52 H. Kato, M. Hori, R. Konta, Y. Shimodaira and A. Kudo, *Chem. Lett.*, 2004, **33**, 1348–1349.